Analytical investigation of all-optical wavelength conversion in a semiconductor-optical-amplifier integrated distributed feedback laser wavelength converter based on four-wave mixing

Hassan Kaatuzian
Mostafa Keshavarz Moazzam*
AmirKabir University of Technology
Electrical Engineering Department
Photonics Research Laboratory
Tehran, Iran
E-mail: hsnkato@aut.ac.ir

Abstract. We investigate nondegenerate four-wave mixing and the resulting high efficiency of wavelength conversion in a semiconductor-optical-amplifier integrated distributed feedback laser, which is one of the latest achievements of photonics technology. For analyzing the amplifier we use a finite-difference beam propagation method based on solution of a modified nonlinear Schrödinger equation, and for the laser we use a coupled-wave approach. We investigated wavelength conversion up to 4-THz pump-probe detuning with lossless conversion up to 400-GHz detuning and a conversion efficiency of −4.8 dB at 1-THz pump-probe detuning. For calibration and verification of the software developed in this study, we have used experimental measurements reported from MIT electronics and Fujitsu research laboratories on a similar device. We have successfully estimated the conversion efficiency of the tested device.
[DOI: 10.1117/1.2832764]

Subject terms: semiconductor optical amplifier; distributed feedback laser; nondegenerate four-wave mixing; finite-difference beam propagation method; coupled-wave theory; conversion efficiency; optical wavelength converter.

Paper 060864RR received Nov. 15, 2006; revised manuscript received Aug. 7, 2007; accepted for publication Aug. 26, 2007; published online Jan. 16, 2008.

1 Introduction

All-optical wavelength conversion is a key technology for wavelength control in ultra-high-speed photonic networks.[1,2] In wavelength division multiplexing (WDM) optical communication systems, among the most important elements are wavelength converters.[1–4] With increasing data communication rates in optical fibers, the demand for faster devices is pressing.[1–6] To design high-speed all-optical wavelength converters, much work has been done, of which one of the best results is the semiconductor optical amplifier (SOA) integrated distributed feedback (DFB) laser.[2,7] Among its excellent features are format-free and broadband wavelength conversion with extremely high conversion efficiency.[2]

In this paper we investigate nondegenerate four-wave mixing (NDFWM) for wavelength conversion in an SOA DFB laser. Our integrated device is a multiple quantum well (MQW) InGaAsP/InP structure with a center wavelength of 1553 nm (Fig. 1). It is composed of three portions[2]: first, the input-side SOA (on the left) for increasing the input signal linear gain; second, the output-side SOA (on the right) for increasing the conversion efficiency; third, a quarterwave-shifted (QWS) DFB laser (in the middle). In order to analyze the SOA portions of this device, we use the finite-difference beam propagation method (FDBPM)[8] based on a modified nonlinear Schrödinger equation.[8,9] Using this method, the wavelength dependence of the gain for detuning larger than 1 THz is obtained.[8]

The central part of the integrated device has a correlative

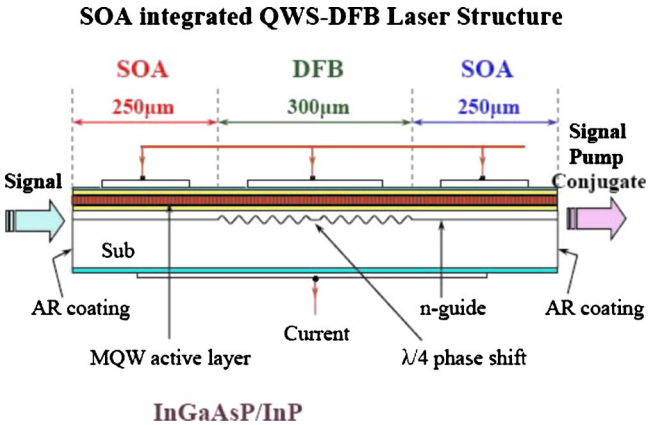

Fig. 1 Schematic diagram of analyzed wavelength converter with SOA portions on both left and right sides and 300-μm-length DFB portion in middle.

*Material presented in this paper is a part of Mostafa Keshavarz Moazzam's work on his thesis towards the MS degree. Dr. Hassan Kaatuzian is his supervisor on the thesis.

0091-3286/2008/$25.00 © 2008 SPIE

structure with a quarterwave shift at the center. It acts as a QWS DFB laser. Using highly nondegenerate four-wave mixing (HNFWM), it can achieve terahertz wavelength conversion. To analyze this central portion, and to evaluate its efficiency, we use a coupled-wave approach.[10,11] The presented coupled-wave model includes rapid intraband effects like carrier heating (CH) and spectral hole burning (SHB) over a defined detuning range in the DFB laser.[10,11]

Using the preceding two models together, we have developed a computer program for simulation of a tested integrated device, and calibration and verification of the program to simulate new devices even before fabrication. The dependence of the conversion efficiency on the coupling coefficient of the DFB laser and the length of the output SOA has been calculated. We have also found that by selecting more appropriate parameters for the integrated device, avoiding gain saturation, we can obtain a device with 5 to 8 dB better conversion efficiency than the mentioned tested devices.

In the next section, an analytical model for SOA portion is explained. The theoretical model for the DFB laser portion is described in Sec. 3. In Sec. 4 we present the results of simulation and a discussion. Section 5 concludes.

2 Analytical Model for the SOA Portion

In order to analyze the two SOAs, which are on opposite sides of the device, we use the FDBPM based on solving a modified nonlinear Schrödinger equation (MNSE).[8,9] In Sec. 2.1 we explain in brief the model for investigating propagation of a single optical pulse in the output-side SOA. Since FWM happens only in the output-side SOA, we specialize our analysis.

2.1 *Propagation of Single Pulse in an SOA*

First, we use the nonlinear Schrödinger equation (derived from the wave equation) for an optical pulse in the slowly varying approximation[8]:

$$\left[\frac{\partial}{\partial z}-\frac{i}{2}\beta_2\frac{\partial^2}{\partial\tau^2}+\frac{\gamma}{2}+\left(\frac{\gamma_{2_P}}{2}+ib_2\right)|V(\tau,z)|^2\right]V(\tau,z)$$
$$=\left\{\frac{1}{2}g_N(\tau)\left[\frac{1}{f(\tau)}+i\alpha_N\right]+\frac{1}{2}\Delta g_T(\tau)(1+i\alpha_T)\right.$$
$$\left.-i\frac{1}{2}\frac{\partial g(\tau,\omega)}{\partial\omega}\bigg|_{\omega_0}\frac{\partial}{\partial\tau}-\frac{1}{4}\frac{\partial^2 g(\tau,\omega)}{\partial\omega^2}\bigg|_{\omega_0}\frac{\partial^2}{\partial\tau^2}\right\}V(\tau,z), \quad (1)$$

where $V(\tau,z)$ is the time-domain complex envelope function of an optical pulse in the local time frame $\tau\,(=t-z/v_g)$; here v_g is the group propagation velocity at the center frequency of the optical pulse. Physically, $|V(\tau,z)|^2$ represents the optical pulse power. On the left side of this equation, β_2 is the group-velocity dispersion (GVD), γ is the linear loss coefficient, γ_{2P} is the two-photon absorption coefficient, $b_2\,(=\omega_0 n_2/cA)$ is the instantaneous self-phase modulation term, $\omega_0\,(=2\pi f_0)$ is the center angular frequency of the pulse, n_2 is the instantaneous nonlinear refractive index, c is the velocity of light in vacuum, and $A\,(=wd/\Gamma)$ is the effective area, where w and d are the width and thickness of the active area, respectively, and $\Gamma$is the confinement factor.

The first term on the right-hand side of Eq. (1) represents the dynamic gain due to carrier density variations (N), where $g_N(\tau)$ and α_N are the saturated gain and the linewidth enhancement factor due to carrier depletion, respectively, $f(\tau)$ is the spectral hole-burning (SHB) function, and $g_N(\tau)$ and $f(\tau)$ are expressed as follows:

$$g_N(\tau)=g_0\exp\left[-\frac{1}{W_s}\int_{-\infty}^{\tau}\exp\left(-\frac{s}{\tau_s}\right)|V(s)|^2\mathrm{d}s\right], \quad (2)$$

$$f(\tau)=1+\frac{1}{\tau_{\mathrm{shb}}P_{\mathrm{shb}}}\int_{-\infty}^{+\infty}u(s)\exp\left(-\frac{s}{\tau_{\mathrm{shb}}}\right)|V(\tau-s)|^2\mathrm{d}s, \quad (3)$$

where g_0 is the unsaturated linear gain, W_s is the saturation energy, P_{shb} is the SHB saturation power, and τ_s and τ_{shb} are the carrier lifetime and the SHB relaxation time, respectively. In the second term of the right side of Eq. (1), which represents gain dynamics due to variations of the carrier temperature, $\Delta g_T(\tau)$ is the gain changes due to the CH and two-photon absorption, and α_T is the linewidth enhancement factor due to the CH; so we have

$$\Delta g_T(\tau)=-h_1\int_{-\infty}^{+\infty}u(s)\exp\left(-\frac{s}{\tau_{\mathrm{shb}}}\right)\left[1-\exp\left(-\frac{s}{\tau_{\mathrm{shb}}}\right)\right]$$
$$\times|V(\tau-s)|^2\mathrm{d}s-h_2\int_{-\infty}^{+\infty}u(s)\exp\left(-\frac{s'}{\tau_{\mathrm{ch}}}\right)$$
$$\times\left[1-\exp\left(-\frac{s}{\tau_{\mathrm{shb}}}\right)\right]|V(\tau-s)|^4\mathrm{d}s, \quad (4)$$

where h_1 is the contribution of stimulated emission and free-carrier absorption to CH gain reduction, h_2 is the contribution of two-photon absorption, and τ_{ch} is the CH relaxation time. Finally, the last two terms of the MNSE, which represent gain and phase dynamic dispersion, respectively, are as follows[9]:

$$\frac{\partial g(\tau,\omega)}{\partial\omega}\bigg|_{\omega_0}=A_1+B_1[g_0-g(\tau,\omega_0)], \quad (5)$$

$$\frac{\partial^2 g(\tau,\omega)}{\partial\omega^2}\bigg|_{\omega_0}=A_2+B_2[g_0-g(\tau,\omega_0)], \quad (6)$$

where

$$g(\tau,\omega_0)=\frac{g_N(\tau,\omega_0)}{f(\tau)}+\Delta g_T(\tau,\omega_0). \quad (7)$$

Here A_1 and A_2 are the slope and the curvature of the linear gain at the central angular frequency ω_0, respectively, and B_1 and B_2 are constants describing the variation of these quantities in saturation conditions. Since in this model the nonlinear Schrödinger equation includes dynamic gain change terms, separating the equation into terms for linear propagation and for phase compensation is impossible, and consequently, numerical solution of the equation using methods like the fast Fourier transform BPM is very difficult.[9] Therefore, we use the FD BPM technique to

simulate the model.[12,13] In this method, the first and second derivatives in the Schrödinger equation are replaced by the central-difference approximation; afterward, the obtained relation is integrated with respect to z (the propagation direction); and finally, the tridiagonal system of simultaneous linear equations is obtained as follows:

$$-a_k(z+\Delta z)V_{k-1}(z+\Delta z)+[1-b_k(z+\Delta z)]V_k(z+\Delta z) - c_k(z+\Delta z)V_{k+1}(z+\Delta z) = a_k(z)V_{k-1}(z)+[1+b_k(z)]V_k(z)+c_k(z)V_{k+1}(z), \quad (8)$$

where $V_k=V(\tau_k)$, $V_{k+1}=V(\tau_k+\Delta\tau)$, and $V_{k-1}=V(\tau_k-\Delta\tau)$; and a_k, b_k, and c_k are the elements of the main diagonal of the tridiagonal matrix, $\Delta\tau$ is the sampling time, k is the number of samples, and Δz is the propagation step. By solving the tridiagonal simultaneous equations (8) at each propagation position z, we can find the complex envelope function of the optical pulse at the next position, $V(z+\Delta z)$. Since the right-side coefficients in Eq. (8) are not determined in each calculation step, we cannot solve it directly. So we should use an iterative approximation technique to solve it.[14,15]

2.2 *Propagation of Three Simultaneous Optical Pulses in the SOA and FWM Portions*

When two optical pulses with different central frequencies f_p (pump) and f_q (probe) are injected into the SOA simultaneously, the FWM signal is generated in the SOA at a frequency $2f_p-f_q$. Now, if a third optical pulse (conjugate signal) with central frequency $f_{cc}=2f_p-f_q$ arrives at the SOA simultaneously with the pump and probe optical pulses, then besides the previously produced signal, another FWM signal will also be produced at the probe central frequency $f_q=2f_p-f_{cc}$. It should be noticed that these two produced FWM signals together amount to further amplification of the output main and amplified probe and conjugate signals. Since in our model, the conjugate signal is much smaller than the pump and probe signals coming into the SOA, the effect of this further amplification can be very important for the conjugate signal frequency. We have used the following equation for describing the three input pulses that are simultaneously injected into the SOA:

$$V(\tau)=V_p(\tau)+V_q(\tau)\exp(-i\,\Delta\omega\,\tau)+V_{cc}(\tau)\exp(i\,\Delta\omega\,\tau), \quad (9)$$

$$\Delta\omega=2\pi\,\Delta f=2\pi(f_p-f_q)=2\pi(f_{cc}-f_p), \quad (10)$$

where $V_p(\tau)$, $V_q(\tau)$, and $V_{cc}(\tau)$ are the complex envelope functions of the input pump, probe, and conjugate pulses, and $\Delta\omega$ is the angular-frequency detuning. In order to estimate the effect of the integrated input SOA on conversion efficiency, we solve Eq. (1) using the combined envelope function (9). The model described in the previous subsection can be used similarly for the output-side SOA.

3 Theoretical Model for the DFB Laser Portion

The model that we utilize for the DFB portion is a coupled-wave model.[10,11] The coupled-wave model is a very useful model based on the wave equation. In this approach, the wave equation for a DFB laser device is written, and after expressing it in terms of different quantities, such as the total intracavity electrical field and the components of the inductive polarization, new equations are obtained, which we can use to estimate how the pump and probe fields interact with each other to produce the conjugate field.[11]

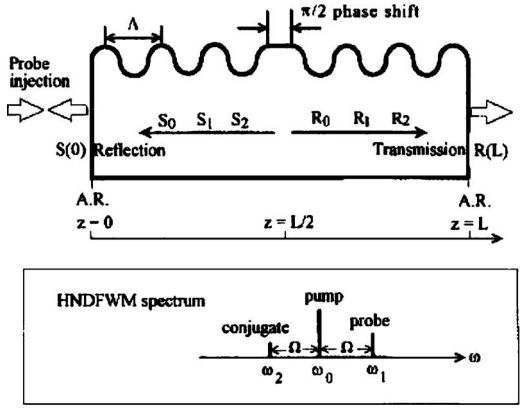

Fig. 2 Schematic diagram of middle QWS DFB portion of device, and pump-signal spectrum.

The scalar wave equation in a DFB laser cavity is as follows:

$$\nabla^2E-\frac{n^2(z)}{c^2}\frac{\partial^2E}{\partial t^2}=\frac{1}{\varepsilon_0c^2}\frac{\partial^2P}{\partial t^2}, \quad (11)$$

where c is the velocity of light in vacuum, ε_0 is the vacuum permittivity, and $n(z)$ is an environment refractive index that has been modulated by a Bragg grating.[16] Here E is the intracavity TE-polarized and normalized electrical field, which for a QWS DFB laser (see Fig. 2 and Ref. 10) is expanded as follows:

$$E(z,t)=\exp(-i\omega_jt)\sum_{j=0,1,2}[R_j(z)\exp(ik_Bz)+S_j(z)\exp(ik_Bz)]+\text{c.c.}, \quad (12)$$

where R_j and S_j are the complex slowly varying envelope functions of the forward and backward fields, respectively; $j=0,1$, and 2 represent the produced inner pump wave in the laser, the probe wave, and the produced conjugate wave due to FWM, respectively; k_B $(=\pi/\Lambda)$ is the Bragg wave number; and Λ is the first-order index grating period.

Using the known relations[11] for $n(z)$ and the polarization P and substituting Eq. (12) into the wave equation, the coupled-wave equations for a DFB laser cavity are obtained:

$$\frac{dR_j}{dz}=\left[\frac{i\omega_j^2\Gamma\chi_j^L}{2k_Bc^2}+\frac{i(k_j^2-k_B^2)}{2k_B}\right]R_j+\frac{i\kappa k_j}{k_B}S_j+\frac{i\omega_j^2\Gamma\chi_j^{\text{FWM}}}{2k_Bc^2E_0^2}(R_0^2R_{3-j}^*+2R_0S_0S_{3-j}^*),$$

$$-\frac{dS_j}{dz}=\left[\frac{i\omega_j^2\Gamma\chi_j^L}{2k_Bc^2}+\frac{i(k_j^2-k_B^2)}{2k_B}\right]S_j+\frac{i\kappa k_j}{k_B}R_j+\frac{i\omega_j^2\Gamma\chi_j^{FWM}}{2k_Bc^2E_0^2}(S_0^2S_{3-j}^*+2R_0S_0R_{3-j}^*), \quad (13)$$

where the boundary conditions at the end facets of DFB are

$$R_1(z=0)=A_{inj},\quad R_2(z=0)=0,\quad S_{1,2}(z=0)=0. \quad (14)$$

After numerically solving the coupled equations (13) under the boundary conditions (14), the transmission and reflection gains of probe and conjugate waves are calculated as follows:

$$Tro_{1,2}=|R_{1,2}(L)|^2/|A_{inj}|^2, \quad (15)$$

$$Ref_{1,2}=|S_{1,2}(0)|^2/|A_{inj}|^2. \quad (16)$$

In the preceding equations ω_j is the angular frequency of the jth wave; Γ is the confinement factor; κ is the DFB coupling coefficient; k_j $(=\bar{n}_j\omega_j/c)$ is the wave number of the jth wave, and $\bar{n}_j$ is its effective mode index; and A_{inj} is the injected field at the angular frequency ω_1.

On the other hand, in Eq. (13), relationships associated with the linear and FWM susceptibilities ($\chi_{1,2}^L$ and $\chi_{1,2}^{FWM}$) for probe and conjugate waves are given as follows[17,18]:

$$\chi_{1,2}^L=-\frac{\bar{n}_{1,2}cG_{1,2}}{\omega_{1,2}}(\beta+i)\left(1-\frac{|E_0|^2/I_s}{1+|E_0|^2/I_s}\mp j\Omega\tau_s\right), \quad (17)$$

$$\chi_{1,2}^{FWM}=\frac{i\bar{n}_{1,2}c}{\omega_{1,2}(1+|E_0|^2/I_s)}\left[\frac{g_{cdp}(1-i\beta)}{1+|E_0|^2/I_s\mp i\Omega\tau_s}+\frac{g_{ch}(1-i\beta_{ch})}{(1\mp i\Omega\tau_1)(1\mp i\Omega\tau_2)}+\frac{g_{shb}(1-\beta_{shb})}{(1\mp i\Omega\tau_2)}\right]\frac{E_0^2}{I_s}, \quad (18)$$

where β, β_{ch}, and β_{shb} are the linewidth enhancement factor and the ratios of the real part to the imaginary part of the FWM susceptibilities due to CH and SHB, respectively; Ω is the angular-frequency detuning between the probe and the pump waves; τ_s, τ_1, and τ_2 are the carrier lifetime and the characteristic times of carrier-phonon and carrier-carrier scattering, respectively; and g_{cdp}, g_{ch}, and g_{shb} are nonlinear gain coefficients for the carrier density pulsation, CH, and SHB, respectively.

In Eqs. (17) and (18), in order to consider asymmetric FWM response due to mismatch between lasing wavelength and spectral gain peak, the parabolic gain approximation $G_{1,2}$ has been used as follows:

$$G_{1,2}=\frac{\bar{g}}{1+|E_0|^2/I_s}\left[1-\frac{(\Omega_0\pm\Omega)^2}{\Delta\omega_g^2}\right], \quad (19)$$

where $\bar{g}$ is the small-signal gain, given by

$$\bar{g}=\frac{2\alpha_{th}L}{\Gamma}\left(\frac{1}{\int_0^L\left(1+\frac{|E_0|^2}{I_s}\right)^{-1}dz}\right). \quad (20)$$

In Eq. (19), $2\Delta\omega_g$ is gain-bandwidth product, and Ω_0 is the angular-frequency mismatch. Equation (20) represents the gain clamping effect, so that the small-signal gain $\bar{g}$ is related to the laser threshold amplitude gain α_{th}. The lasing mode corresponds to the lowest α_{th}. On the other hand, using the coupled-wave formalism[11] and considering a $\pi/2$ phase shift at the grating center, the pump field distribution near the lasing threshold is found, as follows:

$$E_{0,th}\left(z<\frac{L}{2}\right)=\frac{\kappa}{\gamma}\sinh\gamma z\, i\exp(ik_Bz)-\left(\cosh\gamma z-\frac{\alpha_{th}}{\gamma}\sinh\gamma z\right)i\exp(-ik_Bz),$$

$$E_{0,th}\left(z>\frac{L}{2}\right)=\left[\cosh\gamma(L-z)-\frac{\alpha_{th}}{\gamma}\sinh\gamma(L-z)\right]\times i\exp(ik_Bz)-\frac{\kappa}{\gamma}\sinh\gamma(L-z)i\exp(-ik_Bz), \quad (21)$$

where γ is the DFB propagating constant. To obtain an efficient HNFWM in a QWS DFB laser, this portion should always work above its threshold level.

In this study, we used the values listed in Table 2 (Sec. 4.3) to simulate the DFB portion of the proposed integrated device using the model described.[10,11,17,19,20] Also, there is an important point we should make here. Since in our model the injection locking and carrier depletion effects have not been considered, the model cannot describe small detuning (<80 GHz) correctly.

4 Results and Discussion

4.1 *Left Portion (Input-Side SOA)*

The pump pulse in our device is produced in the central DFB portion, internally.[2,21] So, at the input SOA, only a single probe pulse will be injected. No FWM happens in this portion. Therefore, we will only have an amplified version of the probe pulse, without other variations, at the output of the left-side SOA.[22] The shape of input pulse of our model is sech^2 and has a bandlimited Fourier transform. In order to match the other results obtained from simulation and experiment, the duration of the input pulse has been taken as 40 ps.[8] For such a duration, the sampling time should be 62.5 fs and the sampling frequency should be 3.90625 GHz.

The power of the probe pulse has been taken as −22 dBm; in view of its duration, its energy will be 0.25 fJ. With this input energy, the efficiency obtained from the left-side SOA is 3.4 dB, which has been earned without device gain saturation. We should mention that under the same input energy, if the duration of the input probe pulse is made much smaller, the probability of gain saturation will be increased and the obtained efficiency from this portion (and *a fortiori* the full device) will be less than the mentioned amounts.

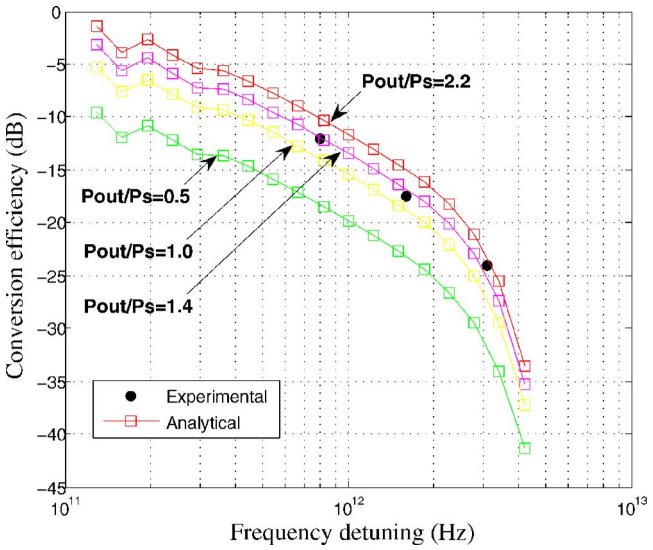

Fig. 3 Analytical and experimental FWM conversion efficiency of an isolated DFB laser versus positive terahertz-range detuning (upward frequency conversion). The squares are analytical results. Solid curves are experimental data.[1,9] As shown, we have a good agreement between simulation and empirical results for $P_{out}/P_s=1.4$.

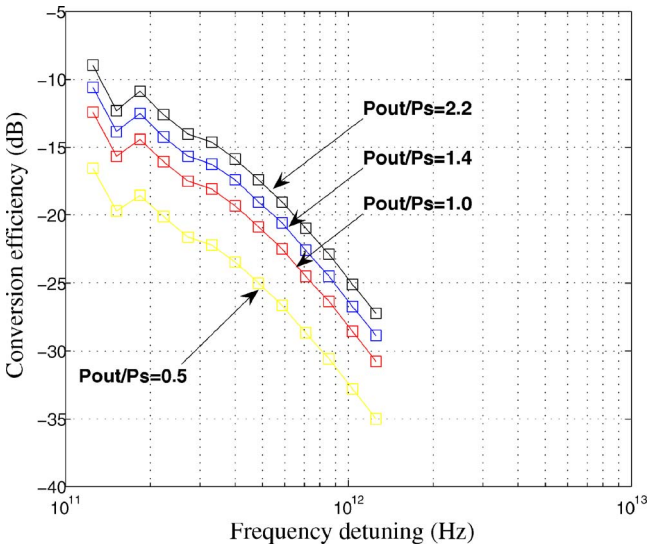

Fig. 4 Conversion efficiency obtained from simulation of the same device as in Fig. 3 in negative detuning (downward frequency conversion).

4.2 *Central DFB Laser Portion*

The described model for the DFB laser is based on solving the coupled-wave equations (13) under the boundary conditions (14). To solve such a two-point boundary-value problem, the best choice is to use an iterative shooting algorithm.[11] In Fig. 3, the conversion efficiency obtained from the model for an isolated DFB laser in positive terahertz-range detuning, $f_p-f_q>0$, is shown. These calculations have been done for a device with small coupling coefficient $\kappa L=0.9$ and for some different output pump power levels P_{outDFB}. In this figure, the obtained results from experimental measurements[2] on a typical device with the same characteristics used in simulation has been shown, too. As shown in Fig. 3, at a normalized pump power level $P_{out}/P_s=1.4$, we have good agreement between simulation and empirical results.

Figure 4 shows the conversion efficiency obtained from simulation of the same device in negative detuning, $f_p-f_q<0$. For output pump power $P_{out}=1.4P_s$, the device conversion efficiency at negative detuning values 300 GHz, 800 GHz, and 1.2 THz are more than 8.3, 11.4, and 13 dB, respectively. The reason for such asymmetry between the positive and negative cases is the competition among the carrier-density pulsation effect, the CH effect, and the SHB effect.[23]

Now, let us return to our own main device. In this case, the optical pulse exiting from the left-side SOA should be injected into the central DFB portion as input. Figure 5 shows the conversion efficiency of a DFB laser device integrated with only one input SOA and also the conversion efficiency of an isolated DFB laser device. For the DFB portion, κL is 1.8. Comparing these two plots implies that the input SOA portion in an integrated device acts only as an input probe pulse amplifier. Indeed, the amount of this amplification, which is 3.4 dB, is the same as the difference between the two curves of Fig. 5. Obviously, an integrated device with longer input SOA length can offer more conversion efficiency; but in a SOA-integrated DFB laser one encounters the gain saturation problem in the output SOA and also the emergence of unfavorable fine structure in the device conversion efficiency. This means that increasing length of the input SOA beyond a certain level will be useless or even harmful.[24,25]

4.3 *Right Portion (Output-Side SOA)*

The output SOA is the most important part of the integrated structure, because it functions both as an optical amplifier and as an optical conjugator. The output of the pump probe and the FWM signal from DFB laser should be injected

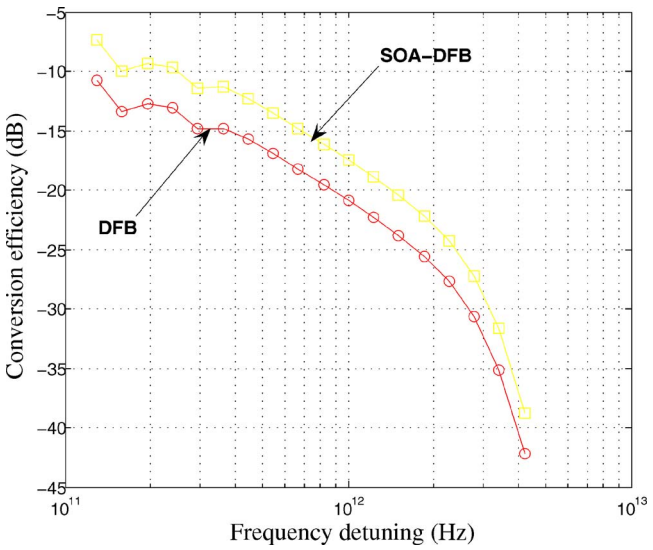

Fig. 5 FWM conversion efficiency of a DFB laser device integrated with only one input SOA (yellow squares) and also that of an isolated DFB laser device (red squares) versus positive detuning. (Color online only).

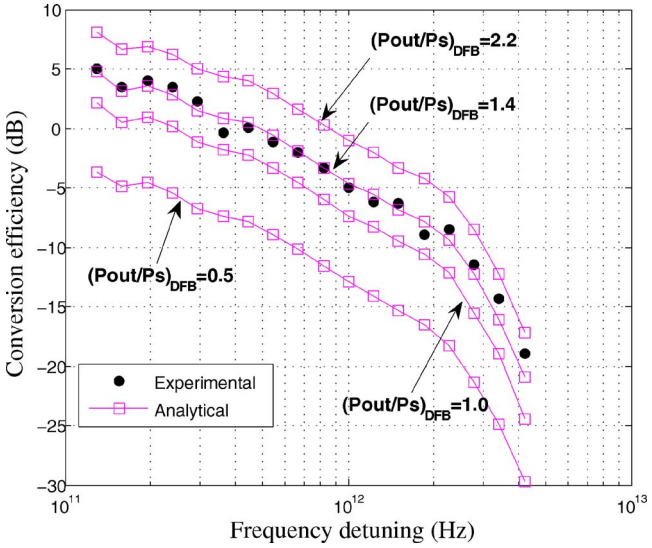

Fig. 6 Analytical and experimental FWM conversion efficiency of a SOA-integrated DFB laser (full device) versus positive detuning. The squares are analytical results, and the solid circles are experimental data.

into this portion. Its performance is analyzed numerically by the FD-BPM method. The duration of each of the three input pulses to this SOA is taken as 40 ps, as in the left-side SOA. The energy of each of these pulses is specified in relation to the output power of the DFB. The input pump pulse energy is taken as fixed and equal to 0.56 pJ.

First, we compare the results obtained from the model with experimental data. To do so, the conversion efficiency obtained from simulation for a full device, versus positive and negative detuning, has been shown with open squares in Figs. 6 and 7, respectively. These results, for a device with $\kappa L = 1.8$ and for various normalized pump power levels (P_{out}/P_s) for the DFB portion, have been calculated. As

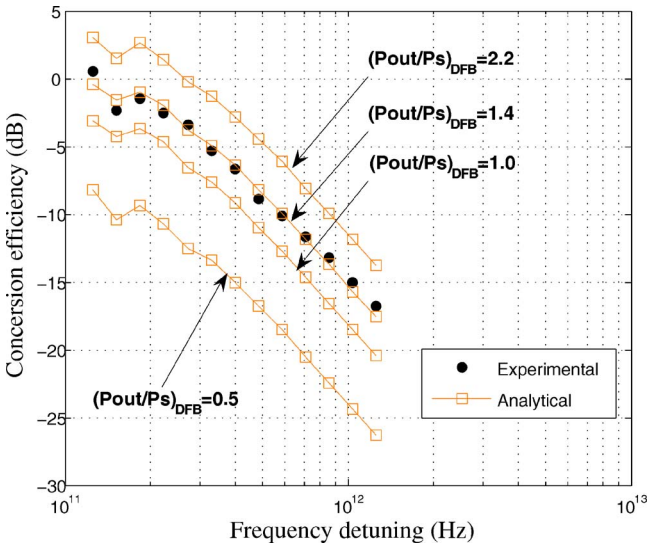

Fig. 7 Analytical and experimental FWM conversion efficiency of a SOA-integrated DFB laser (full device) versus negative detuning. The squares are analytical results, and the solid circles are experimental data.

Table 1 Parameters used in simulation of the SOA portions.

Symbol	Value	Units
L	250	μm
A	0.21	μm^2
f_0	193	THz
g_0	42	cm^{-1}
β_2	0.06	ps^2 cm^{-1}
W_s	65	pJ
α_N	3.4	—
a_T	2.1	—
h_1	0.22	cm^{-1} pJ^{-1}
h_2	114	fs cm^{-1} pJ^{-2}
γ_{2P}	35	cm^{-1} GW^{-1}
τ_s	400	ps
τ_{ch}	650	fs
τ_{shb}	50	fs
P_{shb}	25.5	W
γ	10.5	cm^{-1}
n_2	−0.6	cm^2 TW^{-1}
A_1	0.18	fs μm^{-1}
B_1	−60	fs
A_2	−15	fs^2 μm^{-1}
B_2	0	fs^2

observed, with the listed parameters[2–7,19,25,26] in Tables 1 and 2 and at DFB output pump power $P_{\text{outDFB}} = 1.4P_s$, we can attain the best fit between simulation and experimental results.[1]

It is important to note that this output pump power level for the DFB portion, after being amplified in the output SOA portion, will be 14.6 dBm for the full integrated device output. As we can observe from simulation results, for a typical integrated device,[1] lossless conversion was achieved up to 400-GHz positive detuning; and for higher detuning, the conversion efficiency declines, so that at 1-THz detuning it is −4.8 dB.[1]

In Fig. 8, the conversion efficiency of the full integrated structure with the previously mentioned characteristics (and output pump level $P_{\text{outDFB}} = 1.4P_s$ for the DFB portion), in comparison with an integrated device without output SOA, is shown. We see that the output SOA portion improves the conversion efficiency by 10 to 15 dB. For a positive detuning of 1 THz, the power outputs of the optical pulses from

Table 2 Other parameters used in simulation of the DFB portion.

Symbol	Value	Units
L	300	μm
λ	1553	nm
Γ	0.092	—
I_s	5×10^{10}	W m^{-2}
$\Omega_0/2\pi$	2.2	THz
$2\,\Delta\omega_g/2\pi$	22	THz
β	5.5	—
$\bar{n}_0$	3.4	—
$d\bar{n}/d\omega$	2.4×10^{-16}	s rad^{-1}
g_{cdp}	8.7	cm^{-1}
g_{ch}	9.8	m^{-1}
g_{shb}	16.3	m^{-1}
β_{ch}	14	—
β_{shb}	0.6	—

the right-side SOA, for a full device with input pulse power −22 dBm, are as follows: output pump power: $P_{\text{out-}P}$ =14.6 dBm; output probe power: $P_{\text{out-}q}$=0.2 dBm; FWM signal output power: $P_{\text{out-FWM}}$=−26.6 dBm. From the simulation results and with respect to the obtained energies in the output of the right-side SOA, in the considered detuning range (especially, the output pump energy, which is almost fixed and equals 1.15 pJ), we can easily declare that this part of the integrated device, in present conditions, functions without any gain saturation.

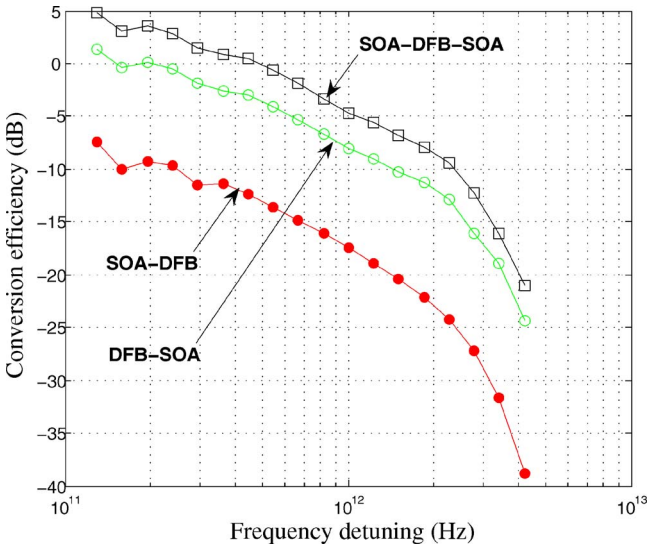

Fig. 8 FWM conversion efficiency versus positive detuning (upward frequency conversion). The squares give the conversion efficiency for the full device. The open and solid circles give the conversion efficiency for an integrated device without the input and output SOAs, respectively.

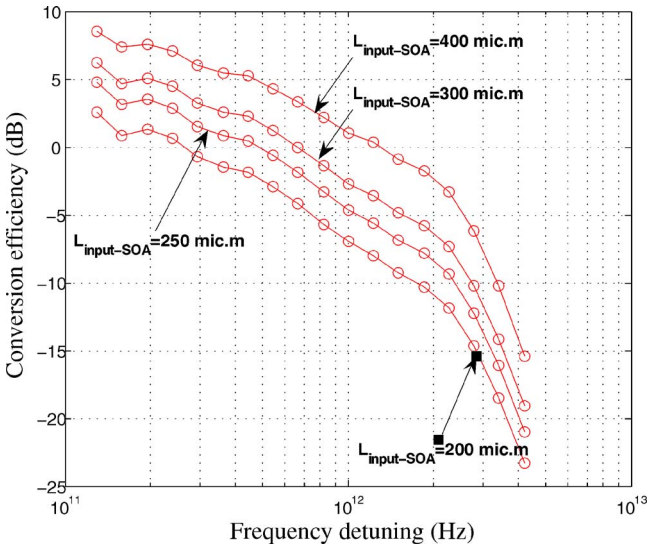

Fig. 9 FWM conversion efficiency of integrated device versus positive detuning for some different lengths of output SOA.

On the other hand, also in Fig. 8 and for comparison, the conversion efficiency of an integrated device without input SOA in the same detuning band has been plotted with open circles. As we expect, the conversion efficiency of the full device is greater, and the difference is 3.4 dB. By comparing the plots in Fig. 8, it is obvious that the output SOA portion has a more important role than the input SOA portion in improving the conversion efficiency; so that for a device with the mentioned features, the output-side SOA increases the conversion efficiency of the integrated device 6.4 times as much as the input-side SOA. This is because in the output SOA portion, two different functions are done synchronously: (1) forming a conjugate signal in output through NDFWM due to interacting pump and probe signals; (2) amplifying the FWM signal from the DFB laser portion for transmission to the right-side SOA portion as input. The preceding cases together make the output SOA have a greater effect in improving the conversion efficiency than the input SOA, which functions only as a probe signal amplifier.

Now, in this section, we repeat our simulation for some different lengths of output SOA; the results are shown in Figs. 9 and 10. As we expect, a longer output SOA causes the device gain to increase, so that for a device with output SOA with length 400 μm, lossless conversion is obtained up to a detuning of 1 THz. But we should note that there are some practical limitations on increasing the SOA length, due to the facet's residual reflectivity. Consequently, with length increasing, a fine structure dependent on wavelength will emerge in the conversion efficiency. So, while designing and testing the laboratory device,[1] this investigation has considered a rather small length for both input and output SOAs.

Another strategy for improving the integrated-device conversion efficiency is concentrating on κL_{DFB} of the cen-

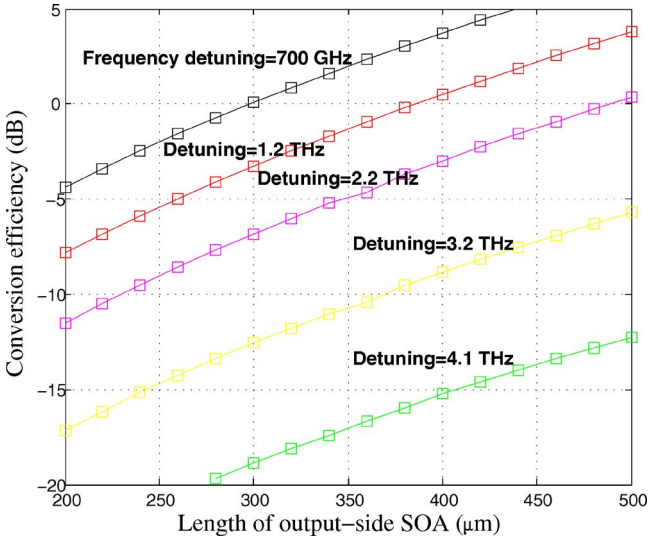

Fig. 10 FWM conversion efficiency of integrated device versus length of output SOA.

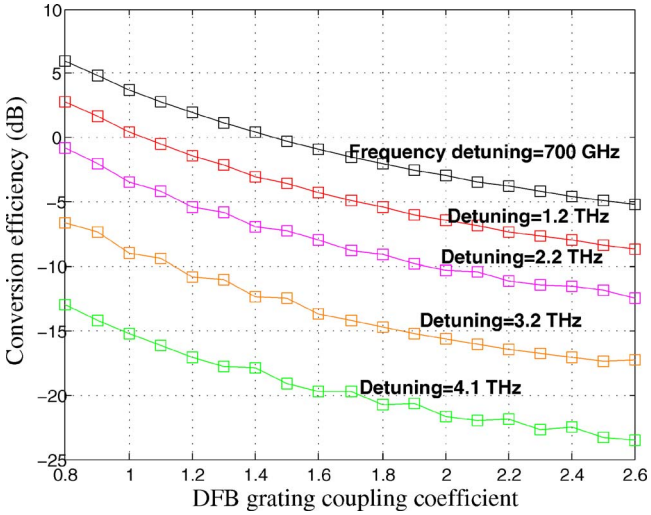

Fig. 12 FWM conversion efficiency of integrated device versus DFB grating coupling coefficient (κL_{DFB}).

tral part (DFB laser). As we know, the grating coupling coefficient in a QWS DFB laser has an important effect on the transmission gain (probe and conjugate) of a device. Figures 11 and 12 present the variations of device conversion efficiency in the favorable detuning range for some medium grating coupling coefficients for the central DFB part. It is observed that decreasing κL_{DFB} increases the conversion efficiency.[7,25] In a DFB laser with smaller κL, the energy coupled to the backward probe and conjugate waves is less, and the forward probe and conjugate waves will transmit more energy to the output face of the DFB laser; so that in our simulation, for a device with $\kappa L_{DFB}=1.0$ for the DFB laser portion, the conversion efficiency is increased by 5.9 dB relative to the reference integrated device (with $\kappa L_{DFB}=1.8$), on average.

It should be noted that for a wavelength converter with a SOA integrated DFB structure, on decreasing the DFB coupling coefficient, not only is the conversion efficiency of this portion increased, but also its probe transmission gain is increased; consequently, the output-side SOA receives more amplified probe power as input. This means that by decreasing κL_{DFB}, the conversion efficiency of the integrated device is increased in two manners. In Fig. 13, the wavelength conversion efficiency is shown for an integrated device with input- and output-side SOA lengths both 350 μm and with $\kappa L_{DFB}=1.5$, and also for another integrated device with input- and output-side SOA lengths 300 μm and $\kappa L_{DFB}=1.1$. The neatly lossless (2.2 dB) wavelength conversion at 1-THz detuning shows promise of practical utility.

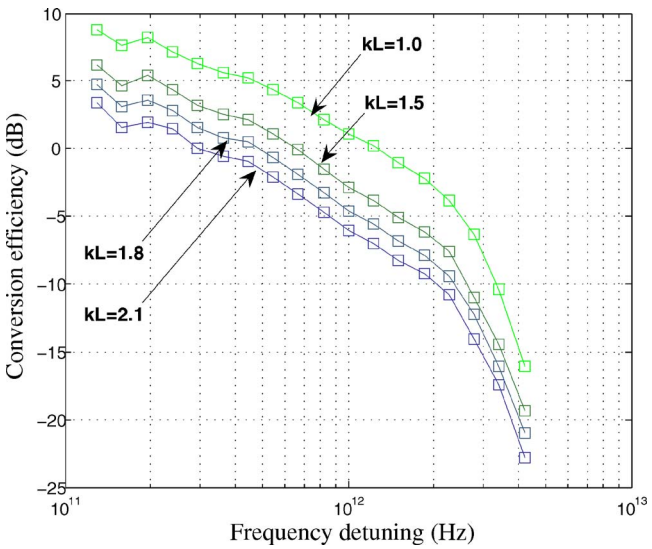

Fig. 11 FWM conversion efficiency of integrated device versus positive detuning for some medium values of the grating coupling coefficients for the central DFB portion.

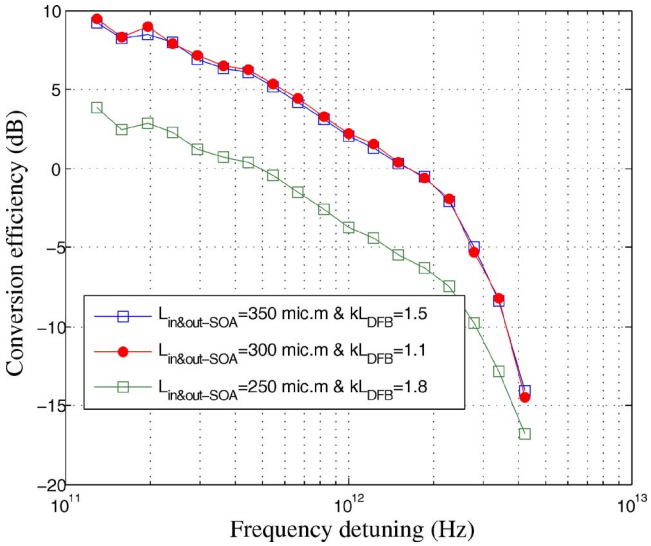

Fig. 13 FWM conversion efficiency of an integrated device with input and output SOA lengths equal to 300 μm and $\kappa L_{DFB}=1.5$ (solid circles), and of another device with input and output SOA lengths 350 μm and $\kappa L_{DFB}=1.1$ (squares).

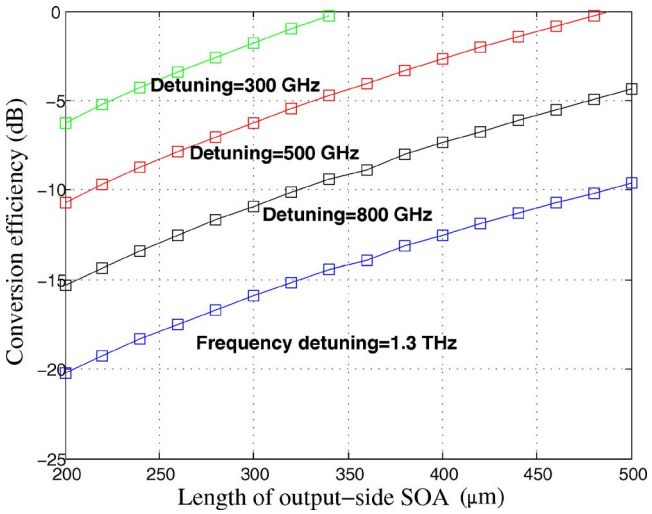

Fig. 14 FWM conversion efficiency of full integrated device versus negative detuning for some different lengths of the output SOA portion.

Finally, we repeated the preceding steps for negative detuning. The results of these simulations and comparisons are presented in Figs. 14 and 15.

5 Conclusion

In this paper, we have presented a numerical analysis of nondegenerate four-wave mixing in the terahertz range for a device consisting of SOAs integrated with a QWS DFB laser. In order to investigate wavelength conversion, in the central λ/4-shifted DFB laser portion we used a coupled-wave approach. We used a finite-difference beam propagation method to analyze the behavior of the two SOA sections that were added to the central part to increase the device conversion efficiency. From the excellent agreement of numerical simulation results with the empirical data, this paper shows quantitatively that our composite model is very useful and robust in analyzing FWM features in such a device. Moreover, the device behavior in wavelength conversion was analyzed at different lengths without any input or output sections. We observed that the conversion efficiency of the integrated device increases with the length of the SOA output section.

We have developed a computer program for analysis of microscopic nonlinear optical wavelength converters. It has now been calibrated and verified using experimental laboratory measurement. It also may predict the signal behavior of such devices at different lengths of the SOA and DFB portions, before fabrication. We hope that our results can improve the design and performance of highly efficient all-optical wavelength converters, wavelength division multiplexers, and especially current WDM systems, which function in optical networks using integrated SOA-DFB wavelength converters.

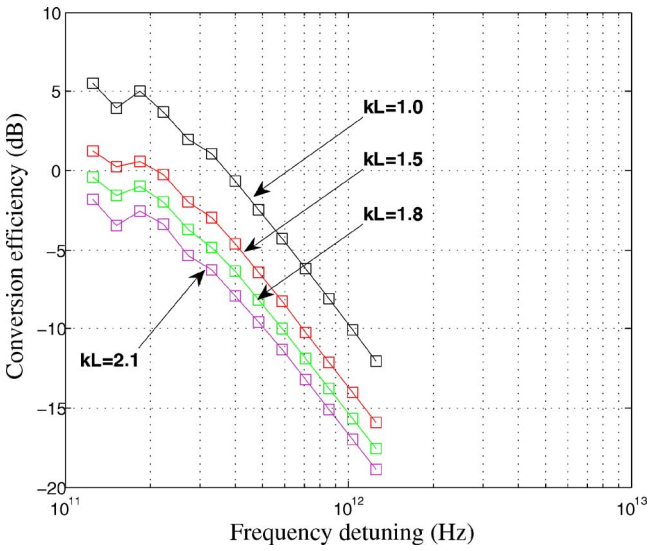

Fig. 15 FWM conversion efficiency of full integrated device versus negative detuning for some medium grating coupling coefficients of the central DFB portion.

References

1. Y. Suzuki and H. Toba, "Recent research and development of all-optical wavelength conversion devices," *NNT Tech. Rev.* **1**, 26–31 (Apr. 2003).
2. T. Simoyama, H. Kuwatsuka, M. Matsuda, Y. Kotaki, and H. Ishikawa, "High-efficiency wavelength conversion using FWM in an SOA integrated DFB laser," *IEEE Photonics Technol. Lett.* **12**, 31–33 (2000).
3. P. M. Gong, J. T. Hsieh, S. L. Lee, and J. Wu, "Theoretical analysis of wavelength conversion based on four-wave mixing in light-holding SOAs," *IEEE J. Quantum Electron.* **40**, 31–40 (Jan. 2004).
4. C. Politi, Q. Klonidis, and M. J. OMahony, "Dynamic behavior of wavelength converters based on FWM in SOAs," *IEEE J. Quantum Electron.* **42**, 108–125 (Feb. 2006).
5. J. T. Hsieh, P. M. Gong, S. L. Lee, and J. Wu, "Improved dynamic characteristics on four-wave mixing wavelength conversion in light-holding SOAs," *IEEE J. Sel. Top. Quantum Electron.* **10**, 1187–1196 (Sep. 2004).
6. C. Politi, D. Klonidis, and M. J. OMahony, "Waveband converters based on four-wave mixing in SOAs," *J. Lightwave Technol.* **24**, 1203–1217 (Mar. 2006).
7. T. Akiyama, H. Kuwatsuka, T. Simoyama, M. Sugawara, and H. Ishikawa, "Design optimisation of SOA-integrated DFB laser wavelength converter," *Electron. Lett.* **38**, 239–241 (Feb. 2002).
8. N. Kumar Das, Y. Yamayoshi, and H. Kawaguchi, "Analysis of basic four-wave mixing characteristics in a semiconductor optical amplifier by the finite-difference beam propagation method," *IEEE J. Quantum Electron.* **36**, 1184–1192 (2000).
9. M. Y. Hong, Y. H. Chang, A. Dienes, J. P. Heritage, P. J. Delfyett, S. Dijaili, and F. G. Peterson, "Femtosecond self- and cross-phase modulation in semiconductor laser amplifiers," *IEEE J. Sel. Top. Quantum Electron.* **2**, 523–539 (1996).
10. J. W. D. Chi, K. Alan Shore, and J. Le Bihan, "Analysis of wavelength conversion using highly nondegenerate four-wave mixing in λ/4-shifted DFB lasers," *IEEE J. Quantum Electron.* **34**, 1861–1866 (1998).
11. J. W. D. Chi, K. Alan Shore, and J. Le Bihan, "Highly nondegenerate four-wave mixing in uniform and λ/4-shifted DFB lasers," *IEEE J. Quantum Electron.* **33**, 2011–2020 (1997).
12. Y. Chung and N. Dagli, "An assessment of finite difference beam propagation method," *IEEE J. Quantum Electron.* **26**, 1335–1339 (Apr. 1990).
13. S. D. Conte and C. de Boor, *Elementary Numerical Analysis: An Algorithmic Approach*, 3rd ed., McGraw-Hill Book Company, Singapore, (1981).
14. K. Okamoto, *Theory of Optical Waveguides*, (in Japanese), Chap. 7, Corona Publishing Co., Tokyo (1992).
15. E. O. Brigham, *The Fast Fourier Transform and Its Applications*, Prentice Hall, Englewood Cliffs, NJ (1988).
16. A. Yariv, *Quantum Electronics*, 3rd ed., Wiley (1989).
17. A. Mecozzi, S. Scotti, A. D'Ottavi, E. Iannone, and P. Spano, "Four-wave mixing in traveling-wave semiconductor amplifiers," *IEEE J. Quantum Electron.* **31**, 689–699 (Apr. 1995).
18. S. Diez, C. Schmidt, R. Ludwig, H. G. Weber, K. Obermann, S. Kindt, I. Koltchanov, and K. Petermann, "Four-wave mixing in semiconductor optical amplifiers for frequency conversion and fast optical switching," *IEEE J. Sel. Top. Quantum Electron.* **3**, 1131–1145 (Oct. 1997).

19. J. Leuthold, M. Mayer, J. Eckner, G. Guekos, H. Melchior, and C. Zellweger, "Material gain of bulk 1.55 μm InGaAsP/InP semiconductor optical amplifiers approximated by a polynomial model," *J. Appl. Phys.* **87**, 618–620 (2000).
20. T. Simoyama, H. Kuwatsuka, and H. Ishikawa, "Cavity length dependence of wavelength conversion efficiency of four-wave mixing in $\lambda/4$-shifted DFB laser," *Sci. Technol. Jpn.* **34**, 235–344 (1998).
21. B. E. Little, H. Kuwatsuka, and H. Ishikawa, "Nondegenerate four-wave mixing efficiencies in DFB laser wavelength converters," *IEEE Photonics Technol. Lett.* **10**, 519–521 (1998).
22. H. Kaatuzian, *Photonics* (in Persian), Vol. I, Amirkabir Univ. (Polytechnic) Press, Tehran (2005).
23. N. Ogasawara and R. Ito, "Longitudinal mode competition and asymmetric gain saturation in semiconductor injection lasers II: theory," *Jpn. J. Appl. Phys.* **27**, 615–626 (1988).
24. C. Politi, D. Klonidis, and M. J. OMahony, "Waveband converters based on four-wave mixing in SOAs," *J. Lightwave Technol.* **24**, 1203–1217 (Mar. 2006).
25. D. Z. Hsu, S. L. Lee, P. M. Gong, Y. M. Lin, S. S. W. Lee, and M. C. Yuang, "High-efficiency wideband SOA-based wavelength converters by using dual-pumped four-wave mixing and an assist beam," *IEEE Photonics Technol. Lett.* **16**, 1903–1905 (Aug. 2004).
26. J. T. Hsieh, P. M. Gong, S. L. Lee, and J. Wu, "Analysis of frequency chirping of optical phase conjugate signals by four-wave mixing in light-holding SOA's," in *Proc. SBMO/IEEE MTT-S Int. Microwave and Optoelectronics Conf.*, pp. 571–576 (2003).

Hassan Kaatuzian is an assistant professor and the head of the Photonics Research Laboratory in the Electrical Engineering Department of Amirkabir University of Technology. He received the BSc and MSc degrees in electrical engineering in 1986 and 1988, respectively, from Sharif University of Technology (Tehran, Iran), and the PhD degree in solid-state electronics in 1994 from Amirkabir University of Technology. He is an IEEE LEOS senior member. He has published more than 50 original scientific and technical papers.

Mostafa Keshavarz Moazzam received an MSc degree in electronics engineering in 2006 from Amirkabir University of Technology (Tehran, Iran). He received a BSc in electrical engineering in 2004 from Azad University (Lahidjan, Iran).